

## Article

# Early and Transient Formation of Highly Acidic pH Spikes in Water Radiolysis under the Combined Effect of High Dose Rate and High Linear Energy Transfer

Md Ibrahim Bepari , Jintana Meesungnoen and Jean-Paul Jay-Gerin \* 

Département de Médecine Nucléaire et de Radiobiologie, Faculté de Médecine et des Sciences de la Santé, Université de Sherbrooke, 3001, 12<sup>ème</sup> Avenue Nord, Sherbrooke, QC J1H 5N4, Canada; md.ibrahim.bepari@usherbrooke.ca (M.I.B.); jintana.meesungnoen@usherbrooke.ca (J.M.)

\* Correspondence: jean-paul.jay-gerin@usherbrooke.ca

**Simple Summary:** Exposure of water to ionizing radiation (e.g., X- or gamma-rays and charged particles such as protons) leads to the rapid formation of hydronium ions,  $H_3O^+$ . The presence of these  $H_3O^+$  ions temporarily renders the irradiated water very acidic. According to previous work, these early acidity spikes strongly depend on radiation beam parameters such as absorbed dose rate and radiation quality (or “linear energy transfer”, LET). In this study, we examine how this transient acidic response evolves under irradiation conditions combining both high-dose-rate and high-LET (i.e., densely ionizing) radiation. Given the crucial role that pH plays in many cellular functions, it is conceivable that the generation of these acidic pH spikes may possibly play a role in the current radiobiological puzzle that seeks to explain the “FLASH effect” in ultrahigh (FLASH) dose rate radio-, proton-, and hadron-therapy, which selectively spares normal tissues while maintaining tumor control.



**Citation:** Bepari, M.I.;

Meesungnoen, J.; Jay-Gerin, J.-P.

Early and Transient Formation of Highly Acidic pH Spikes in Water Radiolysis under the Combined Effect of High Dose Rate and High Linear Energy Transfer. *Radiation* **2023**, *3*, 165–182. <https://doi.org/10.3390/radiation3030014>

Academic Editors: Gérard Baldacchino, Eric Deutsch, Marie Dutreix, Sandrine Lacombe, Erika Porcel, Charlotte Robert, Emmanuelle Bourneuf, João Santos Sousa and Aurélien de la Lande

Received: 16 August 2023

Revised: 6 September 2023

Accepted: 7 September 2023

Published: 11 September 2023

**Abstract:** (1) Background: Water radiolysis leads to the formation of hydronium ions  $H_3O^+$  in less than 50 fs, resulting in the formation of transient acidic pH spikes in the irradiated water. The purpose of this study is to examine the time evolution of these spikes of acidity under irradiation conditions combining both high absorbed dose rate and high-LET radiation. (2) Methods: The early space–time history of the distributions of the various reactive species was obtained using our Monte Carlo multitrack chemistry simulation code IONLYS-IRT. To simulate different LETs, we used incident protons of varying energies as radiation sources. The “instantaneous pulse” (or Dirac) model was used to investigate the effect of dose rate. (3) Results: One major finding is that the combination of high dose rates and high LETs is clearly additive, with a very significant impact on the pH of the solution. For example, at 1 ns and for a dose rate of  $\sim 10^7$  Gy/s, the pH drops from  $\sim 4.7$  to 2.7 as the LET increases from  $\sim 0.3$  to 60 keV/ $\mu\text{m}$ . (4) Conclusions: Confirming previous work, this purely radiation chemical study raises the question of the possible importance and role of these spikes of acidity in underpinning the physical chemistry and biology of the “FLASH effect”.

**Keywords:** water radiolysis; radiation dose rate; linear energy transfer (LET); acidity (pH); Monte Carlo multitrack chemistry simulation; radiation chemical yield (G value); FLASH effect



**Copyright:** © 2023 by the authors. Licensee MDPI, Basel, Switzerland. This article is an open access article distributed under the terms and conditions of the Creative Commons Attribution (CC BY) license (<https://creativecommons.org/licenses/by/4.0/>).

## 1. Introduction

Living cells are composed of a variety of molecules and compounds, with water being the most abundant constituent, accounting for about 70–90% of the cell mass. Therefore, a thorough knowledge of the radiolysis of water is critical for understanding the effects of ionizing radiation on living organisms. When energetic radiation is absorbed by water, it produces chemically reactive species that can damage all biomolecules present in living cells, such as lipids, proteins, and DNA (the so-called “indirect effect” of radiation). Of all biomolecules, DNA is considered the most important in determining the radiobiological

response. Ionizing radiation can randomly induce lesions in cellular DNA, which can either be repaired or result in cytotoxic and mutagenic effects and chromosomal instability that can be detrimental to the organism [1–5]. The severity of the damage caused by ionizing radiation depends on several factors, including the radiation absorbed dose and dose rate, radiation quality (or “linear energy transfer”, LET, also defined as the rate of energy loss per unit path length or “stopping power”,  $-\Delta E/\Delta x$ ), and the presence of radioprotective/antioxidant agents [6–8].

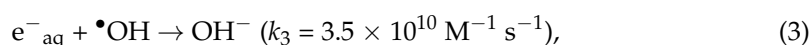
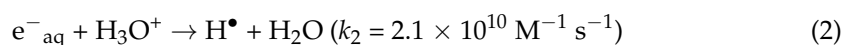
Recently, classical radiobiological principles established during the past century have been challenged by the observation that radiation therapy using ultrahigh dose rates (mean values in excess of  $\sim 40$ – $100$  Gy/s) in short timeframes (milliseconds) selectively spares normal tissues without compromising tumor-killing efficacy. This fascinating new irradiation method in radiotherapy, known as “FLASH-RT” [9,10], results in a markedly increased therapeutic index compared to conventional radiation delivery, which is administered at much lower dose rates ( $\sim 0.03$  Gy/s) and over minutes. Such a FLASH normal-tissue protection effect has become a topic of great value in radiotherapy and its advantages are receiving widespread attention in fundamental and clinical research using electron irradiation, and, more recently, with megavoltage photons and cyclotron-based protons, helium, and even carbon ions (see, e.g., [11–20]). Despite all the work carried out to date, the molecular mechanisms underlying the different responses of tumor and normal tissue to FLASH remain largely unknown.

Following water radiolysis at the prevailing ultrahigh FLASH dose rates (pulses of a fraction of a second), we previously demonstrated with Monte-Carlo-based simulations the existence of strongly acidic spikes which appear transiently over the entire irradiated volume immediately after the passage of the radiation [21,22]. Let us briefly recall here the origin of this acidity.

Upon being ionized into  $\text{H}_2\text{O}^{\bullet+}$ , water molecules undergo rapid dissociation (in times less than  $\sim 50$  fs [23]) via a pseudo-first-order proton transfer reaction to yield the hydronium cation ( $\text{H}_3\text{O}^+$ ) and the hydroxyl radical ( $\bullet\text{OH}$ ) [1,24]:



The  $\text{H}_3\text{O}^+$  and  $\bullet\text{OH}$  produced in reaction (1) are located very close to the position at which ionization occurred. On the other hand, the secondary electron (also called “dry” electron) created during the ionization event is ejected with a kinetic energy of a few tens of electron-volts [25–27], allowing it to travel, on average, a distance of the order of  $\sim 10$  nm [28] before becoming thermalized and hydrated (at about 1.3 ps [29,30]). At this point in time, the hydrated electron ( $e^-_{\text{aq}}$ ), on the one hand, and  $\text{H}_3\text{O}^+$  and the  $\bullet\text{OH}$  radical, on the other hand, are quite far apart [31–33]. Such a situation precludes the possibility of an immediate recombination between these charges according to the following reactions:



where  $k_2$  and  $k_3$  are the rate constants for the two reactions [34]. As a result, this initial charge separation creates a very acidic environment around the “native” radiation track, which will persist until diffusion of the slowly moving  $\text{H}_3\text{O}^+$  and  $\bullet\text{OH}$  has brought these two species to the remote position then occupied by the  $e^-_{\text{aq}}$ , eventually forming  $\text{H}^\bullet$  and  $\text{OH}^-$  through reactions (2) and (3). We previously called this transient acid response an “acid spike” [35,36] in analogy with the “thermal spike” sometimes proposed in radiation chemistry to describe the formation of a transient excess temperature region around the tracks of very-high-LET heavy ions in water [37]. Although experimental evidence of this early acidity has been obtained by several authors [24,38–40], these acid-spike effects have gone largely unnoticed in water exposed to ionizing radiation [41]. From a radiobiological

point of view, this is rather surprising in view of the fact that many biological structures and cellular processes are highly susceptible to variations in pH [41,42].

The spikes of acidity described just above obviously involve individual, nonoverlapping radiation tracks, i.e., they apply only when the dose rates (or, in other words, the densities of absorbed energy) are sufficiently low such that no overlap between the different tracks occurs. In that case, the transient yields and the concentrations of  $\text{H}_3\text{O}^+$  formed by radiolysis are independent of the dose rate, and the acid-spike response is characteristic only of the LET of the radiation [36,43]. Under conditions of high dose rates, however, track overlap starts setting in at a very early stage of radiolysis, with the adjacent tracks overlapping even before the intratrack reactions are completed. At the ultrahigh dose rates of FLASH-RT, the energy of the ionizing radiation can then be considered to be relatively uniformly distributed throughout the entire irradiated volume. As a result, the transient acid spikes around each radiation track combine due to their close physical proximity, thus producing an early acidic pH response across the whole solution [21,22].

Interestingly, these latter results are consistent with the theoretical work of Schneider et al. [44], who applied a kinetic model for water radiolysis to the high-dose-rate regime commonly encountered during liquid cell electron microscope imaging experiments. These authors found that high-dose-rate irradiation indeed strongly alters the concentration of  $\text{H}_3\text{O}^+$  in (aqueous) solutions, estimating that the initial, preirradiation pH of 7 decreased to  $\sim 3.25$  as the dose rate increased to  $\sim 10^{10}$  Gy/s.

In this work, we extend our Monte Carlo track chemistry simulations to study the effect of combining the action of both high absorbed dose rate and high-LET irradiations on the transient yields and concentrations of  $\text{H}_3\text{O}^+$  ions and the resulting acidic pH spikes that form early in water radiolysis, in relation to their potential relevance to the FLASH effect. The present study can thus be seen as a continuation of our previous work [21,22,36].

## 2. Multitrack Chemistry Simulation of High-LET and High-Dose-Rate Effects in Water Irradiated by Fast Incident Protons

### 2.1. Radiolysis of Pure, Deaerated Water: Time Scale of Events and Formation of Primary Radical and Molecular Products

In a condensed phase such as liquid water, the radiolysis products (water cations  $\text{H}_2\text{O}^{\bullet+}$ , excited water  $\text{H}_2\text{O}^*$ , and all ejected secondary electrons) generated in the initial or “physical” stage ( $\sim 1$ – $100$  as) of radiation action [45,46] are very energetically/chemically unstable and undergo a complex sequence of fast reactions and reorganization in the second or “physicochemical” stage ( $\leq 1$  ps), leading to the formation of the very first reactive chemical species which include  $e^-_{\text{aq}}$ ,  $\text{H}_3\text{O}^+$ ,  $\text{OH}^-$ ,  $\text{H}^\bullet$ ,  $\bullet\text{OH}$ ,  $\text{H}_2$ ,  $\text{H}_2\text{O}_2$ ,  $\text{O}(^1D)$ ,  $\bullet\text{O}(^3P)$ ,  $\text{H}^-$ ,  $\text{O}^{\bullet-}$ , etc. [36,47]. Of these,  $\text{H}_3\text{O}^+$ ,  $e^-_{\text{aq}}$ , and  $\bullet\text{OH}$  are produced in the highest concentrations [36]. All these radiolytic species are spatially distributed in a specific, highly nonhomogeneous track structure that strongly depends on the type and energy of the radiation used [24,37,47,48]. In the case of radiations of low LET (such as Compton electrons produced by  $^{60}\text{Co}$   $\gamma$ -rays, fast (e.g., MeV) electrons, or a few hundred MeV protons with typical LET values of  $\sim 0.3$  keV/ $\mu\text{m}$ ) and under conditions of lack of dose-rate effects (no interaction between tracks), the track structure is initially formed by small, well-separated Magee-type “spurs” (clusters of radiolytic species that are approximately spherical in shape) along the path of the incident radiation [49–52]. The third or “chemical” stage ( $> 1$  ps) of the radiolysis process consists of diffusion processes (obeying Fick’s laws of diffusion) and chemical reactions of these reactive species as the tracks develop in time. At  $25^\circ\text{C}$ , the track expansion is essentially complete (i.e., when the spurs on expanding by diffusion touch each other) by  $\sim 0.2$   $\mu\text{s}$  after the first ionization event [53]. At this point in time, the radiation track structure no longer exists and the species that have escaped from spur/track reactions can be regarded as being homogeneously distributed throughout the bulk of the solution (i.e., the system at large). The main reactive species at homogeneity include  $e^-_{\text{aq}}$ ,  $\text{H}^\bullet$ , and  $\bullet\text{OH}$  (the “radical” products) and  $\text{H}_2$  and  $\text{H}_2\text{O}_2$  (the “molecular” products) [24,48,54]. They are often called, though improperly, “primary” species, and their yields—the “primary” or “escape” yields—are given by  $g(e^-_{\text{aq}})$ ,  $g(\text{H}^\bullet)$ ,  $g(\bullet\text{OH})$ ,  $g(\text{H}_2)$ , and  $g(\text{H}_2\text{O}_2)$ , which

are the numbers of molecules formed per 100 eV of radiation energy absorbed by the system (for conversion into SI units: 1 molecule/100 eV  $\approx$  0.10364  $\mu\text{mol/J}$  [48]). Note that the hydroperoxyl radical,  $\text{HO}_2^\bullet$ , or its ionic form  $\text{O}_2^{\bullet-}$ , has also been identified in deaerated water radiolysis, but is normally neglected because it has a very low yield of  $\sim 0.02$  molecule/100 eV [55], which is less than 1% of the other primary radiolytic species. Finally, beyond a few microseconds, the reactions that occur in the bulk solution can usually be described with conventional homogeneous chemistry methods (see, e.g., [56]). The time scale for the various processes occurring in the low-LET radiolysis of deaerated water is given in Figure 1, which is based on a similar figure from Meesungnoen and Jay-Gerin [47].

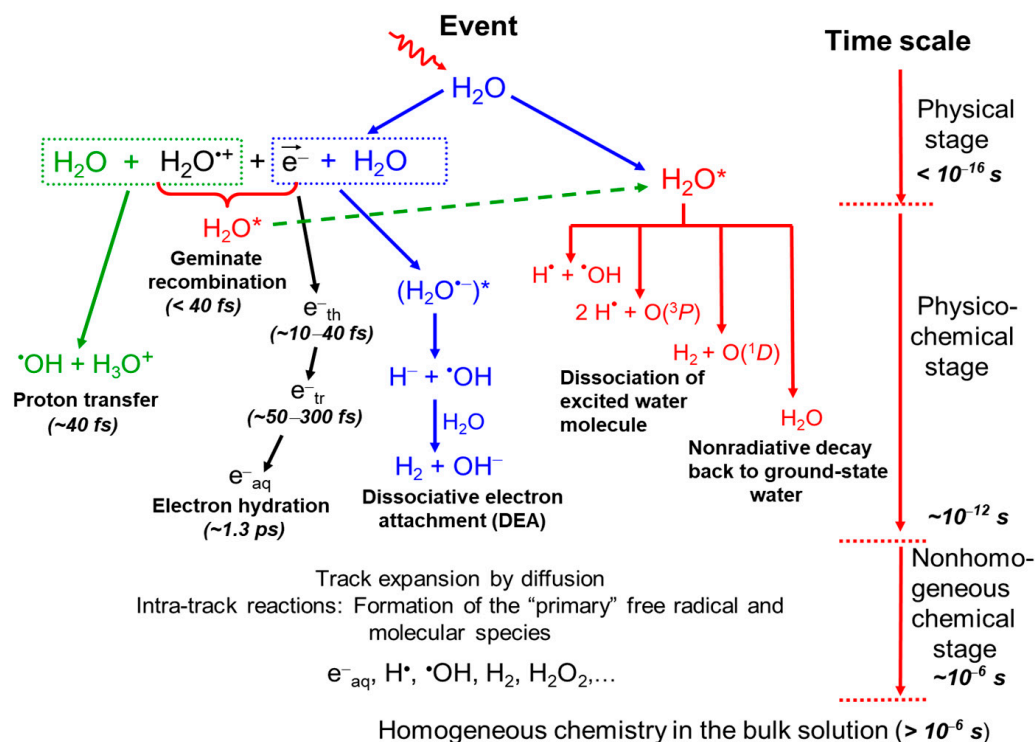


**Figure 1.** Time scale of events in radiolysis of oxygen-free water at low LET. The figure is divided into three, more or less distinct, consecutive, temporal stages: physical, physicochemical, and (nonhomogeneous and homogeneous) chemical, as suggested by Platzman [45] and Kuppermann [46].

## 2.2. Simulating the Effect of LET with Incident Protons of Different Energies

At low LET, tracks are clearly separated initially into spherical spurs that develop independently as time progresses. The adjacent spurs are so far apart that there is practically no overlapping among reactants. Under these conditions, the predominant effect is radical production. With increasing LET, the isolated spur structure changes to a situation in which the spurs are so close to each other that they eventually merge (due to diffusion of the reactive species) along the radiation path, then forming a dense continuous column (cylindrical in shape) of species [37,47,52,57]. This allows more radicals to be formed in close proximity with a correspondingly greater probability of radical–radical combination/recombination reactions during the track stage of radiolysis. Unlike low-LET radiation, where the radical yield is high, densely ionizing radiation therefore tends to increase the yield of the molecular products (such as  $\text{H}_2$  and  $\text{H}_2\text{O}_2$ ) and to reform water.

In this study, to simulate on a quantitative basis the effect of LET on the yields of  $\text{H}_3\text{O}^+$  ions that form early in water radiolysis via reaction (1), we used incident protons of five different energies as radiation sources, namely, 5, 1.5, 0.7, 0.4, and 0.25 MeV, whose mean LET values at 25 °C are  $\sim 8, 19.5, 33, 47,$  and  $60$  keV/ $\mu\text{m}$ , respectively [58–60]. Data for 300 MeV irradiating protons, which mimic the low-LET limit of  $\sim 0.3$  keV/ $\mu\text{m}$  of Compton

electrons ejected from the absorption of  $^{60}\text{Co}$   $\gamma$  rays in liquid water [61], are also used here as a reference.

### 2.3. Modeling the Effect of Dose Rate: The “Instantaneous Pulse” (or Dirac) Model

Herein, a multitrack irradiation model recently formulated in our laboratory was applied to describe the effects of high dose rates on the radiolysis of water by incident protons at ambient [22,62–64] and elevated [65] temperatures. In short, this model consists of the random irradiation of water with single pulses of  $N$  incident monoenergetic protons, which simultaneously impact the water perpendicularly across the surface of a circle of radius  $R_0$  (see Figure 1 of Alanazi et al. [62]). This is the so-called “instantaneous pulse” (or Dirac) model, in which the pulse duration is assumed to be zero [66], i.e., all chemical species are created instantaneously. In this case, the absorbed dose per pulse is the only relevant parameter.

The fact that the fast protons have essentially rectilinear trajectories makes it possible to define a cylindrical geometry of the beam at the entry time, with all proton tracks parallel to the cylinder axis. Since the irradiated cylinder is embedded in nonirradiated bulk water, the various radiolytic species initially formed therein are not confined to this volume, but, rather, diffuse through the entire bulk water (infinite in fact) as time progresses. In this particular irradiation geometry, the incident “fluence” of protons (number of impacting protons per unit area) is simply given by  $N/\pi R_0^2$ , so that the effect of the dose rate can be studied simply by varying  $N$ , the number of irradiating protons per pulse. In the present study,  $N$  is chosen to vary from 1 to 20. Data for  $N = 1$ , which indicates the absence of dose-rate effects, serve as a reference. According to our previous calibration of  $N$  in terms of dose rate (see Figure 3B of Alanazi et al. [62]),  $N = 20$  corresponds to an absorbed dose rate of about  $10^7$  Gy/s. Finally, time zero is chosen as the time when the  $N$  incident protons reach the front of the cylinder.

### 2.4. Monte Carlo Multitrack Chemistry Simulations: The IONLYS-IRT Code

In this work, we use an extended multitrack chemistry version of our Monte Carlo computer code IONLYS-IRT [47] to simulate the radiolysis of pure, deaerated water at 25 °C by incident protons of various energies (i.e., of different LETs) under high-dose-rate conditions. This version has been described in detail elsewhere [22,62,64,65].

In short, we modified our “IONLYS” step-by-step program [67], which covers the early physical and physicochemical stages of radiation action (up to  $\sim 1$  ps), to simulate the space-time history of  $N$  simultaneously incident proton tracks in close spatial proximity [62]. The resulting complex spatial distribution of the reactants of the considered track system then serves directly as the starting point for the subsequent chemical stage ( $>1$  ps), which is covered by our “IRT” program [68]. Using the “independent reaction times” (IRT) method [69,70], this program generates reaction times without having to follow the diffusive trajectories of all the reacting species. Its ability to provide reliable time-dependent chemical yields under a wide range of irradiation conditions has been well validated by comparison with Monte Carlo simulations of full random flights that do follow reactant trajectories in detail [71,72]. It has been shown that simulating  $N$  interactive proton trajectories at the same time does not present any particular problem for the implementation of our IRT program at high dose rates. The only drawback is that the computation times are obviously much longer than for the simulation of single-proton irradiation.

For pure, deaerated water at 25 °C, the reaction scheme, rate constants, and the diffusion coefficients of reactive species used in our IRT program are the same as those used previously [34,58,62,68,73,74].

All calculations were performed by simulating short track segments (typically  $\sim 1$ – $100$   $\mu\text{m}$ , depending on  $N$  and LET) of incident monoenergetic protons having LETs in the range 0.3–60 keV/ $\mu\text{m}$ . For a given value of  $N$  (between 1 and 20) and LET, the number of simulated “histories” (i.e., the number of pulses, usually  $\sim 2$ – $150$ ) was chosen so that

the average chemical yields could be calculated with acceptable statistical reliability while keeping reasonable computer time limits.

### 3. Results and Discussion

#### 3.1. Time Evolution of the Yields of $\text{H}_3\text{O}^+$ and $\text{OH}^-$ in the Absence of Dose-Rate Effects

Figure 2 shows the temporal variation of the yields of  $\text{H}_3\text{O}^+$  and  $\text{OH}^-$  as obtained from our track chemistry simulations of the radiolysis of pure, deaerated water by 300 MeV irradiating protons (LET  $\sim 0.3 \text{ keV}/\mu\text{m}$ ) at ambient temperature, under conditions of lack of dose-rate effects (i.e., one single-proton irradiation,  $N = 1$ ). For comparison, available experimental data for  $^{60}\text{Co}$   $\gamma$ -ray or fast electron irradiation [40,75–78] are also shown in the figure. As can be seen, our simulated values agree very well with the measured  $\text{H}_3\text{O}^+$  and  $\text{OH}^-$  yields. This good agreement between simulated and measured yield values (without adjustable parameters) supports, a posteriori, the validity of the assumptions used in our computational approach and also demonstrates the robustness of our Monte Carlo code to adequately describe the geometry of the proton track structure and its chemical development.

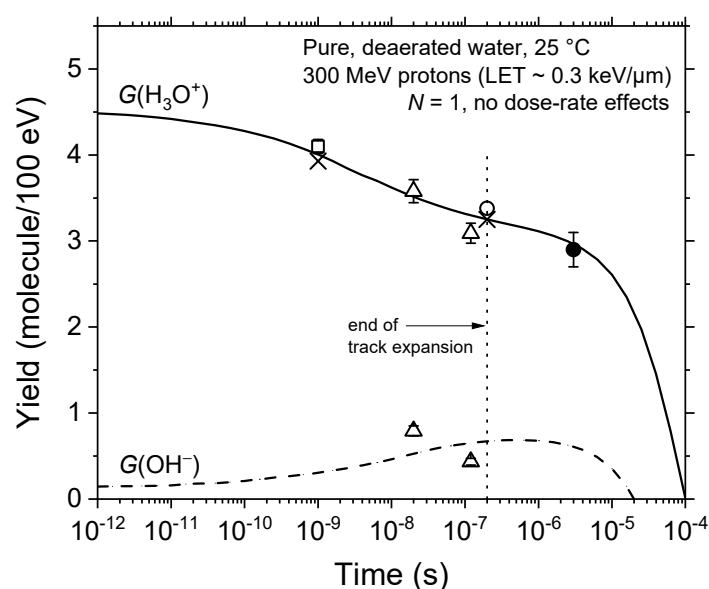


**Figure 2.** Time evolution of the yields (in molecule per 100 eV) of radiolytically produced hydrogen ions,  $G(\text{H}_3\text{O}^+)$  (solid line), and hydroxide ions,  $G(\text{OH}^-)$  (dashed line), obtained from our Monte Carlo simulations of the radiolysis of pure, deaerated water by 300 MeV incident protons (LET  $\sim 0.3 \text{ keV}/\mu\text{m}$ ) at 25 °C, in the interval of  $\sim 1 \text{ ps}$  to  $100 \mu\text{s}$ . Experimental data for  $^{60}\text{Co}$   $\gamma$ /fast electron irradiation: (x) Čerček and Kongshaug [75], (o) Barker et al. [76], (□) Pikaev et al. [40], (Δ) Anderson et al. [77], and (●) Schmidt and Ander [78]. The thin vertical (dotted) line shown at  $\sim 0.2 \mu\text{s}$  indicates the end of spur/track expansion (in the absence of dose-rate effects), i.e., the time marking the end of the nonhomogeneous radiation chemical stage (or, in other words, the transition from nonhomogeneous track kinetics to homogeneous kinetics in the bulk solution) [53].

#### 3.2. Temporal Variation of the Yields of $\text{H}_3\text{O}^+$ and $\text{OH}^-$ under Irradiation Conditions Combining Both High-Dose-Rate and High-LET Radiation

In Figure 3a–f, we compare the effect of dose rate (by varying  $N$ , the “number of proton tracks per pulse”, between 1 and 20) on the time evolution of  $G(\text{H}_3\text{O}^+)$  and  $G(\text{OH}^-)$ , as obtained from our IONLYS-IRT multitrack chemistry simulations of the radiolysis of pure, deaerated water by the six irradiating protons under consideration, whose mean LET values at 25 °C are  $\sim 0.03, 8, 19.5, 33, 47,$  and  $60 \text{ keV}/\mu\text{m}$ , in the interval of  $1 \text{ ps}$ – $10 \mu\text{s}$ . The data obtained for  $N = 1$  (i.e., one single-proton irradiation) are shown for reference.

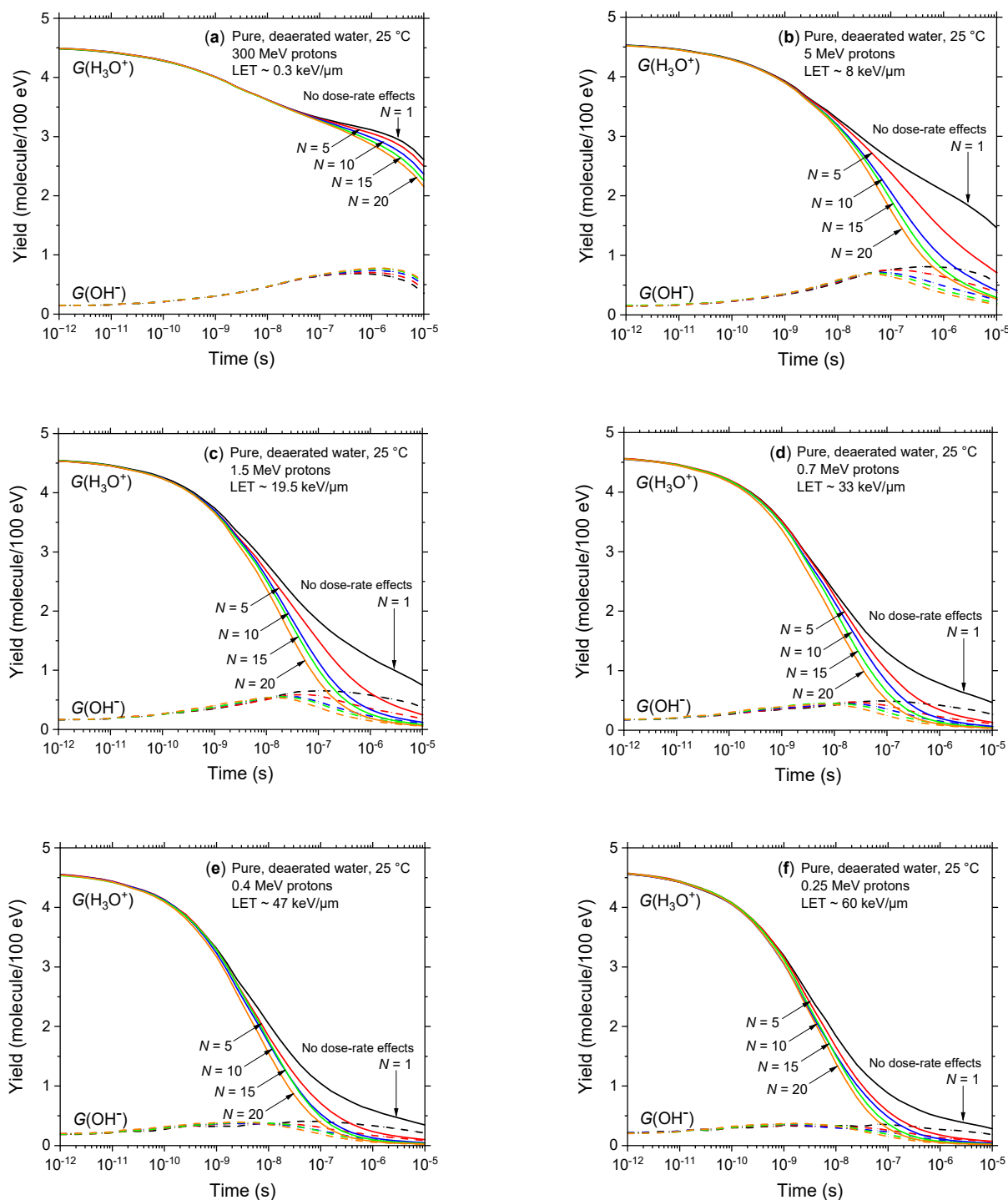
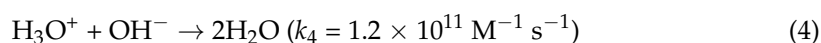


**Figure 3.** Calculated yields (in molecule per 100 eV) of radiolytically produced  $\text{H}_3\text{O}^+$  (solid lines) and  $\text{OH}^-$  (dashed lines) ions as functions of time, LET, and  $N$  (the number of irradiating protons per pulse), obtained from our Monte Carlo multitrack chemistry simulations of the radiolysis of pure, deaerated water by incident protons of varying energies: 300 MeV (LET~0.3 keV/ $\mu\text{m}$ ) (panel (a)), 5 MeV (LET~8 keV/ $\mu\text{m}$ ) (panel (b)), 1.5 MeV (LET~19.5 keV/ $\mu\text{m}$ ) (panel (c)), 0.7 MeV (LET~33 keV/ $\mu\text{m}$ ) (panel (d)), 0.4 MeV (LET~47 keV/ $\mu\text{m}$ ) (panel (e)), and 0.25 MeV (LET~60 keV/ $\mu\text{m}$ ) (panel (f)) at 25 °C, in the interval of ~1 ps to 10  $\mu\text{s}$ . The values of  $N$  chosen to illustrate the dose-rate effects vary from 1 to 20, with  $N = 20$  corresponding to an absorbed dose rate of about  $10^7$  Gy/s (Alanazi et al. [62]). Data for  $N = 1$  correspond to the absence of dose-rate effects and are shown here as a reference.

While the radiolytic formation of  $\text{H}_3\text{O}^+$  causes the irradiated volume to become temporarily acidic, the hydroxide ion  $\text{OH}^-$ , which is formed largely by the ( $e^-_{\text{aq}} + \bullet\text{OH} \rightarrow \text{OH}^-$ ) reaction (3) during the track stage of the radiolysis, contributes to the generation of an early, transient alkaline response, which may therefore counteract the “acid spike” effect discussed in this work. However, as can be seen in the figures,  $G(\text{OH}^-)$  remains much lower than  $G(\text{H}_3\text{O}^+)$  over the entire time range of interest, regardless of the values of  $N$  and the LET considered. As a result, it affects the quantitative features of the pH (see *infra*) only slightly and can be ignored to a reasonably good approximation.

As expected, the yields of  $\text{H}_3\text{O}^+$  (and those of  $\text{OH}^-$ ) are nearly the same at  $\sim 1$  ps irrespective of the LET and of the dose rate. With increasing time,  $G(\text{H}_3\text{O}^+)$  decreases sharply. As can be seen in the figures, this decrease strongly depends on the LET; as the LET increases from  $\sim 0.3$  to  $60 \text{ keV}/\mu\text{m}$ , the decrease in  $G(\text{H}_3\text{O}^+)$  becomes more pronounced as a function of time and begins at shorter times. As discussed previously [36], this decrease is mainly due to  $\text{H}_3\text{O}^+$  reacting with  $\text{OH}^-$  via reaction (4):



and, but to a lesser extent, with  $e^-_{\text{aq}}$ , via reaction (2). Other reactions, such as  $\text{H}_3\text{O}^+ + \text{O}^{\bullet-} \rightarrow \bullet\text{OH} + \text{H}_2\text{O}$  and  $\text{H}_3\text{O}^+ + \text{HO}_2^- \rightarrow \text{H}_2\text{O}_2 + \text{H}_2\text{O}$ , also contribute to the decay of  $G(\text{H}_3\text{O}^+)$  with time but only very weakly. This is illustrated in Figure 4a–f, where we compare the time profiles of the extents  $\Delta G(\text{H}_3\text{O}^+)$  of the various components of  $G(\text{H}_3\text{O}^+)$  calculated from our Monte Carlo multitrack simulations of the radiolysis of deaerated water by 300, 5, and  $0.25 \text{ MeV}$  incident protons (LET  $\sim 0.3, 8,$  and  $60 \text{ keV}/\mu\text{m}$ , respectively) for  $N = 1$  and  $20$ . As can be seen, the contribution of the ( $\text{H}_3\text{O}^+ + \text{OH}^- \rightarrow 2\text{H}_2\text{O}$ ) reaction (4) increases strongly with increasing LET and dose rate and becomes largely predominant in the decay of  $G(\text{H}_3\text{O}^+)$ . This reflects the increasing intervention of intratrack (when the LET increases at a fixed  $N$ ) and intertrack (when  $N$  increases at a fixed LET) radical–radical ( $e^-_{\text{aq}}$  and  $\bullet\text{OH}$  in the present case) reactions in the solution, as the proximity conditions that would allow these radicals to combine or recombine are favored. This results in the formation of more and more  $\text{OH}^-$  in the nonhomogeneous stage of radiolysis, which in turn increases the chance for hydroxide ions to react with  $\text{H}_3\text{O}^+$  on the time scale considered in this work. This explains the faster decay kinetics of  $G(\text{H}_3\text{O}^+)$ , which are observed with increasing LET and dose rate (see Figure 3a–f). To our knowledge, there are no experimental data available in the literature with which to compare our results on the time dependence of the yield of  $\text{H}_3\text{O}^+$  at high LET.

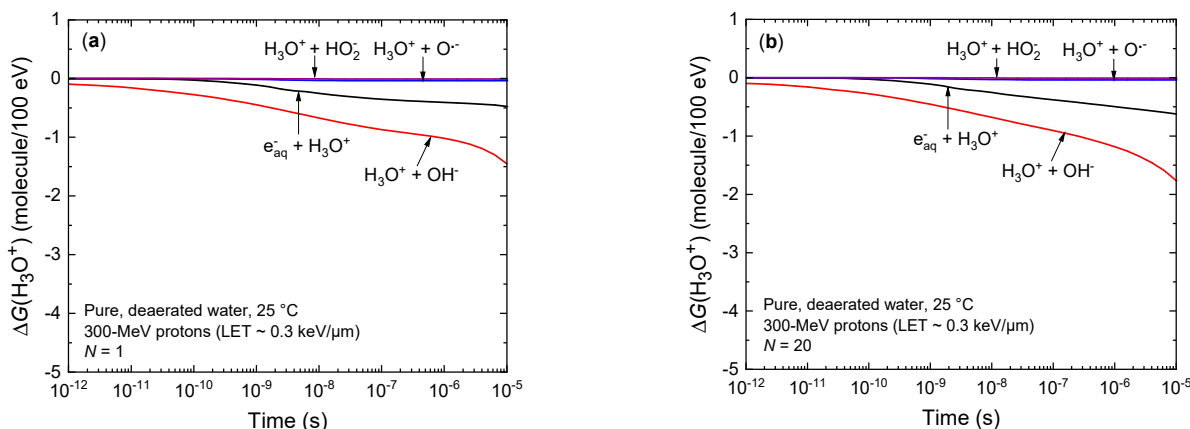
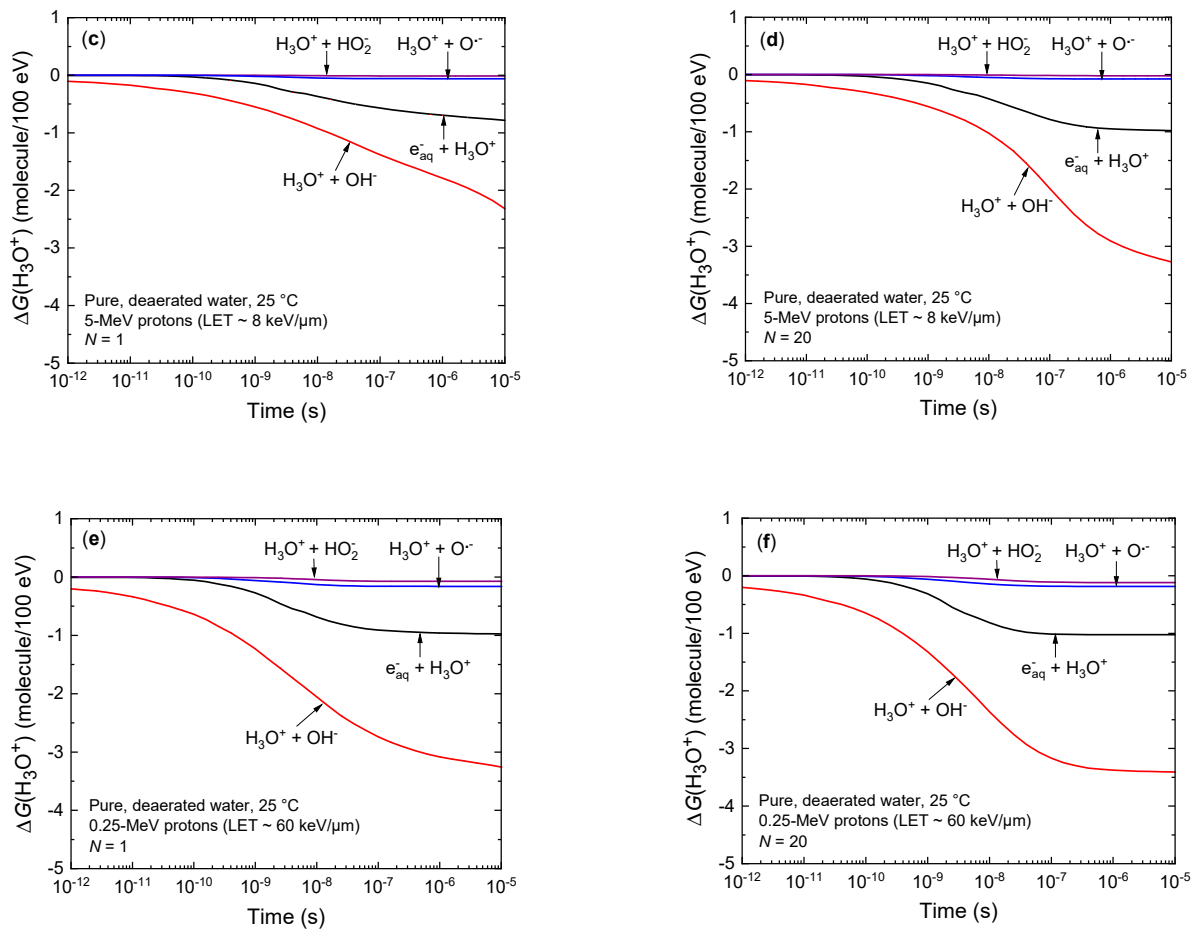


Figure 4. Cont.



**Figure 4.** Time dependence of the cumulative yield variations  $\Delta G(\text{H}_3\text{O}^+)$  (in molecule per 100 eV) for each of the reactions that contribute to the yield of  $\text{H}_3\text{O}^+$  on the  $\sim 1$  ps– $10$   $\mu\text{s}$  time scale, calculated from our Monte Carlo simulations of the radiolysis of pure, deaerated water by incident protons of different energies and dose rates (see text): 300 MeV (LET $\sim 0.3$  keV/ $\mu\text{m}$ ) for  $N = 1$  (panel (a)) and  $N = 20$  (panel (b)), 5 MeV (LET $\sim 8$  keV/ $\mu\text{m}$ ) for  $N = 1$  (panel (c)) and  $N = 20$  (panel (d)), and 0.25 MeV (LET $\sim 60$  keV/ $\mu\text{m}$ ) for  $N = 1$  (panel (e)) and  $N = 20$  (panel (f)) at 25 °C. The value of  $N = 20$  chosen here to illustrate the dose-rate effects corresponds to an absorbed dose rate of  $\sim 10^7$  Gy/s (Alanazi et al. [62]). Data for  $N = 1$  (i.e., for one single-proton track) correspond to the absence of dose-rate effects and are shown as a reference.

### 3.3. The Onset of Dose-Rate Effects

As can be seen in Figure 3a–f, for all the LET values considered, the different  $G(\text{H}_3\text{O}^+)$  curves initially remain unchanged as a function of time regardless of  $N$ , until a critical time ( $\tau_c$ ) is reached, after which the different yield values begin to deviate from their respective one single-proton irradiation ( $N = 1$ ) reference curves. This critical time, which clearly depends on  $N$ , can be regarded as a signature for the “onset” of dose-rate effects in the solution as a whole [62,65,79]. In other words,  $\tau_c$  corresponds to the minimum time before interactions between tracks occur. At a given LET, with increasing  $N$ , these deviations occur at ever shorter times and with a greater amplitude. To determine  $\tau_c$ , we used the same method as that developed in Alanazi et al. [62], consisting of (1) subtracting the  $G(\text{H}_3\text{O}^+)$  vs. time values that correspond to the simulation of  $N$  ( $=5, 10, 15,$  and  $20$  in the present case) interacting proton tracks from those obtained for  $N = 1$  (i.e., under conditions of lack of dose-rate effects), and (2) noting the time when this difference (initially near zero, as the yield curves are all superimposed) begins to increase. Figure 5 compares the variation of our values of  $\tau_c$  so determined as a function of  $N$  in a log–log plot for different LET values, namely,  $\sim 0.3, 8, 33,$  and  $60$  keV/ $\mu\text{m}$ . As shown in the figure, there is

a similar linear relationship between the logarithms of  $\tau_c$  and  $N$  for the four LET values considered, with the corresponding straight lines being practically all parallel. However, Figure 5 shows that the straight lines obtained for the three high-LET 5, 0.7, and 0.25 MeV irradiating protons ( $\sim 8$ , 33, and 60 keV/ $\mu\text{m}$ , respectively) nearly coincide (within their plotting accuracy) and are shifted by about two decades (two orders of magnitude) to shorter times compared with that obtained for irradiation with low-LET 300 MeV incident protons ( $\sim 0.3$  keV/ $\mu\text{m}$ ) [62]. Qualitatively, this result can be explained on physical grounds as it reflects differences in the geometry of the proton track structure: with increasing LET of the radiation, the isolated, well-separated spherical spurs change into dense continuous cylindrical tracks. This favors, at shorter time scales, an increased amount of intervening intratrack reactions. In this high-LET case, the decrease in  $G(\text{H}_3\text{O}^+)$  is therefore expected to begin at shorter times (as compared to the low-LET case) [36]. Quantitatively, Figure 5 shows that  $\tau_c$  remains relatively little dependent on the LET of the irradiating protons in the studied range between  $\sim 8$  and 60 keV/ $\mu\text{m}$ , indicating that the variation of  $\tau_c$  with  $N$  in this LET range is rather insensitive to the track structure and is mainly controlled by the intertrack interactions (i.e., by the distances between neighboring tracks).

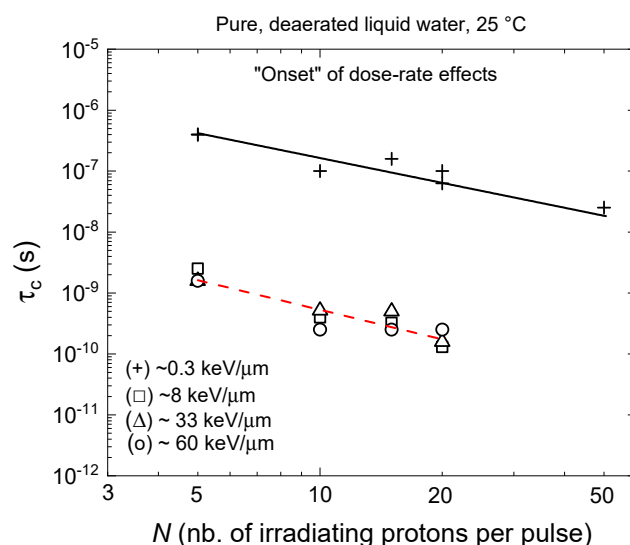


**Figure 5.** Log–log plot showing the variation of the time  $\tau_c$  (in second) at which intertrack interactions (or dose-rate effects) start to occur in the radiolysis of deaerated, pure water by 300 MeV (LET $\sim 0.3$  keV/ $\mu\text{m}$ ) (+), 5 MeV (LET $\sim 8$  keV/ $\mu\text{m}$ ) (□), 0.7 MeV (LET $\sim 33$  keV/ $\mu\text{m}$ ) (Δ), and 0.25 MeV (LET $\sim 60$  keV/ $\mu\text{m}$ ) (o) incident protons at 25 °C, as a function of  $N$ , the “number of incident protons per pulse” in our cylindrical irradiation model (see text). The two straight lines were obtained from a least-squares fit of the different  $\log(\tau_c)$  vs.  $\log(N)$  data: the solid black line is from data for 300 MeV irradiating protons, and the dashed red line is from the combined data for 5, 0.7, and 0.25 MeV incident protons.

According to the results of Figure 5, the linear relationship that is observed between the logarithms of  $\tau_c$  and  $N$  (i.e., the dose rate) can be written as

$$\tau_c = \frac{\text{constant}}{(N)^n}, \quad (5)$$

where the constant of proportionality depends on the LET of the radiation, and the 99% confidence interval of the exponent contains the value  $n \approx 1$  [62,65]. In other words, it can be concluded that, whatever the proton LET values considered in this work,  $\tau_c$  varies inversely with the dose rate.

### 3.4. Ultrafast, Transient Acidic pH Response

In order to calculate the pH values prevailing in the solutions, we now need to estimate the concentrations of the radiolytically generated hydronium ions,  $[\text{H}_3\text{O}^+]_{\text{radiolytic}}$ , as a function of time. This can readily be carried out by using our calculated  $G(\text{H}_3\text{O}^+)$  values reported in Figure 3a–f with the general relationship [80]

$$C = \rho DG, \quad (6)$$

where  $C$  is the concentration,  $\rho$  is the density of the solution,  $D$  is the radiation dose, and  $G$  is the chemical yield. Using our cylindrical, multitrack irradiation model (see Section 2.3) and assuming that the hydronium ions generated by  $N$  incident protons are evenly distributed in the considered circular cylinder with a length of  $1 \mu\text{m}$  and initial radius  $R_0 = 0.1 \mu\text{m}$  (at 1 ps; see Figure 1 of Alanazi et al. [62]),  $[\text{H}_3\text{O}^+]_{\text{radiolytic}}$  (expressed in millimolar, mM) can be derived from [47,62,81,82]

$$[\text{H}_3\text{O}^+]_{\text{radiolytic}}(t) \approx 5.3 \times 10^{-6} \times \left( \frac{N \times \text{LET}}{R(t)^2} \right) \times G(\text{H}_3\text{O}^+)(t), \quad (7)$$

where LET is in  $\text{keV}/\mu\text{m}$ ,  $G(\text{H}_3\text{O}^+)$  is in molecule per 100 eV, and

$$R(t)^2 \approx R_0^2 + 4D(\text{H}_3\text{O}^+)t \quad (8)$$

represents the change of  $R_0$  (in  $\mu\text{m}$ ) over time due to the two-dimensional diffusive expansion of the tracks. Here,  $t$  is the time (in s) and  $D$  ( $=9.46 \times 10^{-9} \text{ m}^2 \text{ s}^{-1}$  [73]) is the diffusion coefficient of  $\text{H}_3\text{O}^+$  in water.

The total concentration of  $\text{H}_3\text{O}^+$  in the solution is thus the sum of  $[\text{H}_3\text{O}^+]_{\text{radiolytic}}$  given by Equations (7) and (8) and of the nonradiolytic, preirradiation concentration  $[\text{H}_3\text{O}^+]_{\text{autoprotolysis}}$  ( $10^{-7} \text{ M}$  in the present case) due to the autoprotolysis of water:

$$[\text{H}_3\text{O}^+]_{\text{total}}(t) = [\text{H}_3\text{O}^+]_{\text{radiolytic}}(t) + [\text{H}_3\text{O}^+]_{\text{autoprotolysis}}. \quad (9)$$

The pH of the irradiated volume is then simply given by

$$\text{pH}(t) = -\log_{10}([\text{H}_3\text{O}^+]_{\text{total}}(t)). \quad (10)$$

Figure 6a–f shows the temporal evolution of the pH values calculated from Equations (7)–(10) for  $N$  300, 5, 1.5, 0.7, 0.4, and 0.25 MeV irradiating protons in deaerated, pure water at  $25 \text{ }^\circ\text{C}$  for  $N = 1, 5, 10, 15,$  and  $20$ , using the  $G(\text{H}_3\text{O}^+)$  values given in Figure 3a–f. As can be seen, for all LET values considered, there is an abrupt transient acid pH effect at times immediately after the initial energy deposition. This “acid spike” effect is found to be most intense at times shorter than, say,  $\sim 1\text{--}10 \text{ ns}$ . In this time range, the pH remains nearly constant, decreasing markedly with the LET of the incident radiation. Moreover, its magnitude and duration also strongly depend on the value of  $N$  (i.e., the dose rate). For example, at  $\sim 1 \text{ ns}$ , the pH for 300 MeV incident protons ( $\text{LET} \sim 0.3 \text{ keV}/\mu\text{m}$ ) varies from  $\sim 6.1$  for  $N = 1$  (no dose-rate effects) to  $\sim 4.9$  for  $N = 20$ . For an LET of  $\sim 60 \text{ keV}/\mu\text{m}$ , the pH at  $\sim 1 \text{ ns}$  decreases from  $\sim 4$  for  $N = 1$  to  $\sim 2.7$  for  $N = 20$ . Beyond  $\sim 1\text{--}10 \text{ ns}$ , the pH gradually increases over time in all cases and eventually reaches the constant value of 7 (corresponding to the pH of neutral water at  $25 \text{ }^\circ\text{C}$ ), i.e., when the pH of the solution equals  $-\log_{10}([\text{H}_3\text{O}^+]_{\text{autoprotolysis}})$  according to Equations (9) and (10).

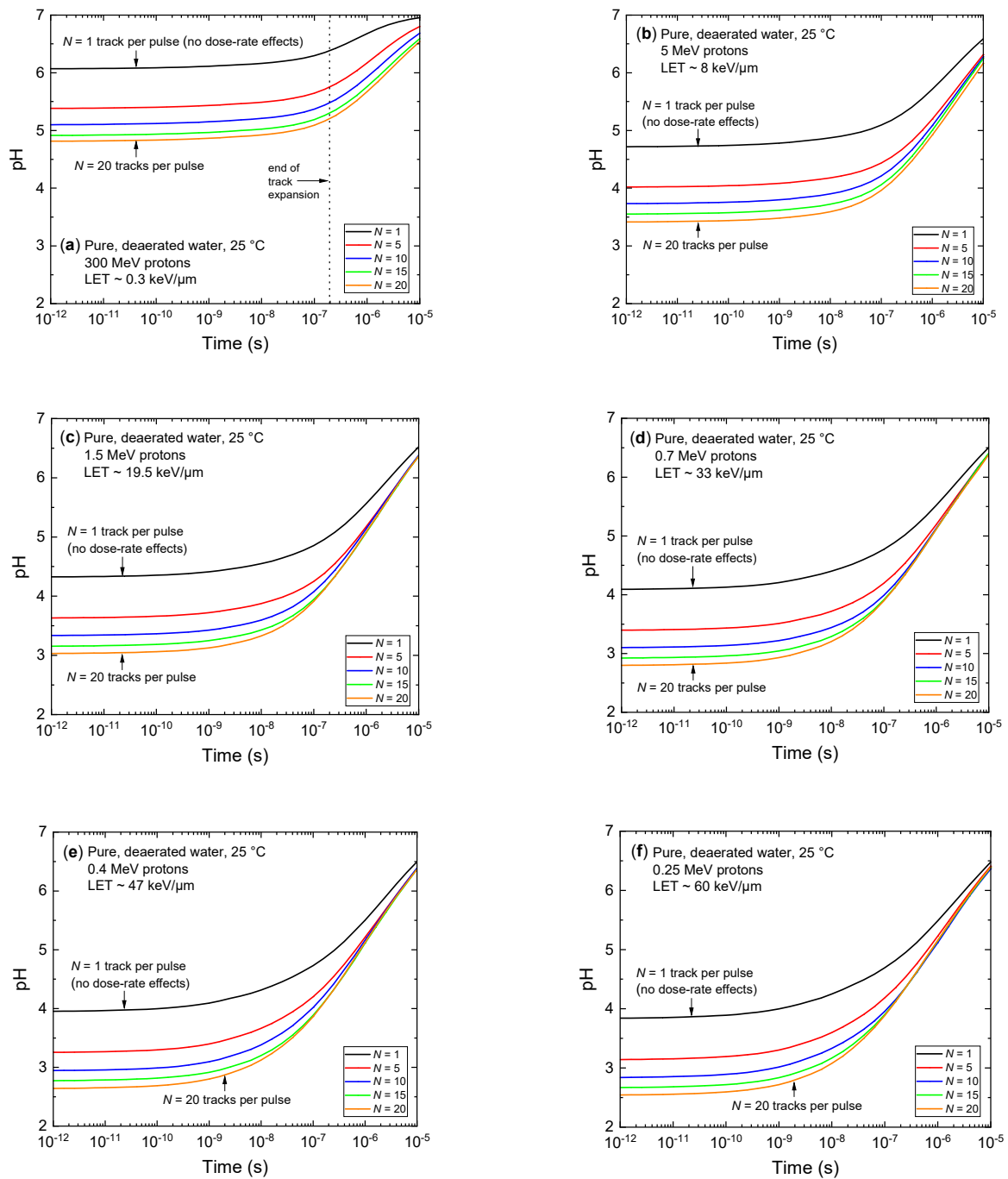


**Figure 6.** Time evolution of pH calculated from Equations (7)–(10) for pure, deaerated water irradiated by protons of varying energies: 300 MeV (LET~0.3 keV/ $\mu\text{m}$ ) (panel (a)), 5 MeV (LET~8 keV/ $\mu\text{m}$ ) (panel (b)), 1.5 MeV (LET~19.5 keV/ $\mu\text{m}$ ) (panel (c)), 0.7 MeV (LET~33 keV/ $\mu\text{m}$ ) (panel (d)), 0.4 MeV (LET~47 keV/ $\mu\text{m}$ ) (panel (e)), and 0.25 MeV (LET~60 keV/ $\mu\text{m}$ ) (panel (f)) at 25 °C, in the interval of  $\sim 1$  ps to  $10 \mu\text{s}$ . The values of  $N$  chosen to illustrate the dose-rate effects vary from 1 to 20, with  $N = 20$  corresponding to an absorbed dose rate of about  $10^7$  Gy/s (Alanazi et al. [62]). Data for  $N = 1$  (i.e., for one single-proton track) correspond to the lack of dose-rate effects and are shown as a reference. The thin vertical (dotted) line shown at  $\sim 0.2 \mu\text{s}$  in panel (a) indicates the end of spur/track expansion, i.e., the time marking the end of the nonhomogeneous radiation chemical stage [53].

### 3.5. Correlation between pH, LET, and Dose Rate

Even though their underlying mechanism of action differs, high dose rates and high LETs obviously deserve special consideration as they affect radiolysis yields in a similar

way: indeed, the probability of radical–radical reactions is increased in both cases, either in the bulk of the solution through intertrack reactions (for high dose rates) or in the individual radiation tracks through intratrack reactions (for high-LET irradiations) [24,62,79,83]. This is theoretically a consequence of the higher radical densities in the track stage of the radiolysis for densely ionizing radiations and/or under conditions of high dose rates. As seen above for irradiating protons, this similarity in the action of high LETs and high dose rates in the radiolysis of water is also well demonstrated here in the  $G$  value for the formation of  $\text{H}_3\text{O}^+$  at early time (see Figure 3a–f) and in the acid pHs that result therefrom (see Figure 6a–f).

For the sake of illustration, Figure 7 shows semi-log plots of the pH against LET for various dose rates ( $N = 1, 10, \text{ and } 20$ ) (panels (a) and (b)) and against  $N$  for various LETs ( $\sim 0.3, 8, 33, \text{ and } 60 \text{ keV}/\mu\text{m}$ ) (panels (c) and (d)) at two different times (1 ps and 1 ns) after the initial energy deposition. As can be seen, a linear correlation is found in both cases, which can be expressed by the following relationships:

$$\text{pH} = A - B \ln(\text{LET}) \text{ where } A \text{ is a function of } N \quad (11)$$

and

$$\text{pH} = E - F \ln(N) \text{ where } E \text{ is a function of LET.} \quad (12)$$

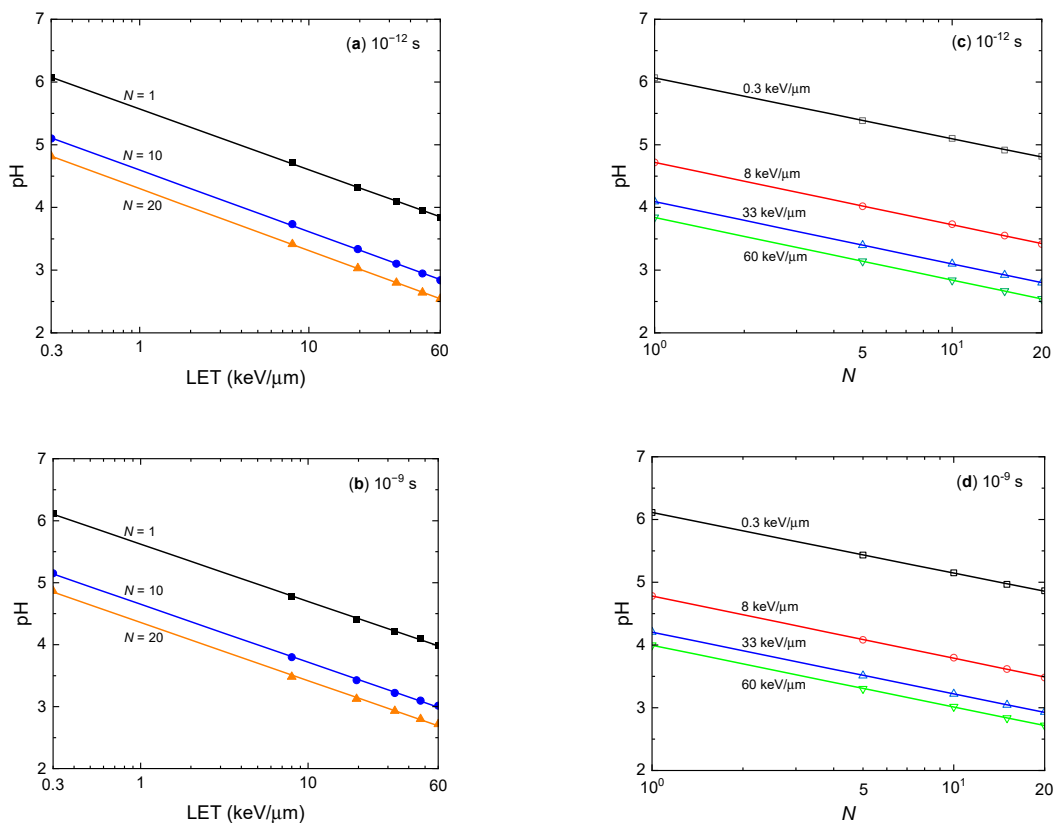


**Figure 7.** Plot of pH against LET for pure, deaerated water irradiated by protons of varying energies: 300 MeV (LET $\sim$ 0.3 keV/ $\mu$ m), 5 MeV (LET $\sim$ 8 keV/ $\mu$ m), 1.5 MeV (LET $\sim$ 19.5 keV/ $\mu$ m), 0.7 MeV (LET $\sim$ 33 keV/ $\mu$ m), 0.4 MeV (LET $\sim$ 47 keV/ $\mu$ m), and 0.25 MeV (LET $\sim$ 60 keV/ $\mu$ m) at 25 °C, at two different times after the initial energy deposition:  $\sim$ 1 ps (panel (a)) and 1 ns (panel (b)). Dose-rate effects are illustrated by three values of  $N$ , the “number of incident protons per pulse”, namely, 1, 10, and 20. Similarly, panels (c,d) show, at the same two times, the plot of pH against  $N$  ( $N = 1, 5, 10, 15, \text{ and } 20$ ) for four different values of the LET:  $\sim$ 0.3, 8, 33, and 60 keV/ $\mu$ m. A clear correlation is observed between pH, LET, and  $N$  (see text).

It should be noted that the parameters  $B$  in Equation (11) and  $F$  in Equation (12), which are, respectively, the slopes of the pH vs.  $\ln(\text{LET})$  and pH vs.  $\ln(N)$  straight lines in Figure 7, do not depend on  $N$  (for  $B$ ) or on the LET (for  $F$ ) since these lines are all parallel (i.e., they have the same slopes whatever the values of  $N$  or of the LET). Indeed, values of these slopes, obtained from a least-squares fit of the pH vs.  $\ln(\text{LET})$  and pH vs.  $\ln(N)$  data and averaged over the two considered times, are  $B = 0.41 \pm 0.02$  ( $A$  varying from  $\sim 5.6$  for  $N = 1$  to  $\sim 4.3$  for  $N = 20$ ) and  $F = 0.42 \pm 0.01$  ( $E$  varying from  $\sim 6.1$  for  $\text{LET} \sim 0.3 \text{ keV}/\mu\text{m}$  to  $\sim 3.9$  for  $\text{LET} \sim 60 \text{ keV}/\mu\text{m}$ ).

#### 4. Conclusions

In this work, we extended our Monte Carlo track chemistry simulations to study the effect of combining the action of both high absorbed dose rate and high-LET irradiations on the transient yields and concentrations of  $\text{H}_3\text{O}^+$  ions and the resulting acid pH spikes that develop at early times during the radiolysis of pure, deaerated water. Using incident protons of varying energies in the range of 300–0.25 MeV as radiation sources to simulate the effect of LET and our previously formulated cylindrical, “instantaneous pulse” (or Dirac) irradiation model to investigate the effect of dose rate, a major finding was that the combination of high dose rates and high LETs is clearly additive, with a very significant impact on the pH of the irradiated solution.

Indeed, for all LET values considered, we observe an abrupt, transient, highly acidic pH response immediately after the initial energy deposition that persists for periods of more than five orders magnitude across the entire solution. The magnitude of this response not only depends on the LET of the radiation but also on the value of its dose rate. For example, at  $\sim 1 \text{ ns}$ , the pH for an LET of  $\sim 0.3 \text{ keV}/\mu\text{m}$  (300 MeV incident protons) varies from  $\sim 6.1$  in the absence of dose-rate effects to  $\sim 4.9$  for an instantaneous dose rate of  $\sim 10^7 \text{ Gy/s}$ . On the other hand, for an LET of  $\sim 60 \text{ keV}/\mu\text{m}$  (0.25 MeV incident protons), the pH at  $\sim 1 \text{ ns}$  decreases from  $\sim 4$  for one single irradiation track to  $\sim 2.7$  for a dose rate of  $\sim 10^7 \text{ Gy/s}$ . At longer times, the pH gradually increases for all LET and dose-rate values, eventually reaching the constant value of 7, which corresponds to the nonradiolytic, preirradiation concentration of hydronium ions, due to the autoprotolysis of water.

This work confirms previous experimental and theoretical studies on the similarity of the action of high dose rates and high LETs in the track stage of the radiolysis. Such a similarity, which manifests itself in the various radiolysis yields, including those of the formation of  $\text{H}_3\text{O}^+$ , finds its origin in an increase in the radical densities. Even if their underlying mechanism of action differs, the probability of radical–radical combination or recombination reactions is increased, either in the bulk of the solution through intertrack reactions (case of high dose rates) or in the individual radiation tracks through intratrack reactions (case of high LETs), with the consequence of an increase in molecular yields and a simultaneous reduction in the radical yields.

Using the space–time history of the tracks, we were able to determine the critical time  $\tau_c$  corresponding to the “onset” of dose-rate effects in the solution. Interestingly, we demonstrated that the variation of  $\tau_c$  with the dose rate is rather insensitive to the track structure (i.e., to the LET of the radiation), but is mainly controlled by the intertrack interactions or, in other words, by the distances between neighboring tracks. Under the conditions of our simulation model, we found that this onset of dose-rate effects is nearly inversely proportional to the dose rate.

To the best of our knowledge, these early acidic pH responses have largely gone unnoticed in water or in a cellular environment exposed to ionizing radiation. In view of the importance of the pH for many cellular functions (e.g., it is well known that the acidity of the intracellular water strongly influences most of the enzyme functions present in the cells), the present findings raise the question of whether the generation of such spikes of acidity in cell water under high-LET and high-dose-rate irradiation conditions plays a role in relation to the “FLASH effect” in FLASH radio-, proton-, and hadron-therapy. This question is all the more relevant when we consider that the diffusion of  $\text{H}_3\text{O}^+$  in cell water

is ~100 to 1000 times lower than in free water [84,85]. In this case, this decrease in mobility of hydronium ions in the water of the cell should then lead to a marked increase in the period of time during which the highly acidic pH spikes are observed, further underlining the potential importance and role of pH in the FLASH effect.

Although this study is based on a *pure radiation chemistry perspective*, we hope that the current findings involving high-LET radiation delivered at high dose rates may provide some useful information for a better understanding of the early physicochemical steps in the chain of radiobiological events that underlie the FLASH effect.

Currently, we are continuing our present modeling work by trying to progress towards the study of a *cellular medium*, including its many various components. In particular, we are working to introduce the effect of the viscosity of intracellular water on the radiolysis and its consequences on the observed acidity spikes. With regard to the effect of acidity itself, we also wish to introduce the effect of quenching of the  $\text{H}_3\text{O}^+$  ions produced by radiolysis by various buffers (e.g., phosphate buffer and others). All these works are in progress.

**Author Contributions:** Conceptualization: J.-P.J.-G., J.M. and M.I.B.; M.I.B. performed all the simulations, analyzed the results, and wrote the original draft of the manuscript based on discussions with J.M. and J.-P.J.-G.; J.M. developed the software and implemented the model; J.M. and J.-P.J.-G. supervised the work; J.-P.J.-G. and M.I.B. reviewed and edited the final version of the manuscript; project administration and funding acquisition: J.-P.J.-G. All authors have read and agreed to the published version of the manuscript.

**Funding:** This research was funded by the Natural Sciences and Engineering Research Council of Canada (NSERC), grant number RGPIN-2022-03972.

**Institutional Review Board Statement:** Not applicable.

**Informed Consent Statement:** Not applicable.

**Data Availability Statement:** Data generated or analyzed during this study are provided in full within the article.

**Acknowledgments:** M.I.B. is the recipient of an Abdenour-Nabid, MD graduate scholarship from the “Programme de bourses d’excellence aux études supérieures” of the Université de Sherbrooke.

**Conflicts of Interest:** The authors declare no conflict of interest.

## References

1. von Sonntag, C. *Free-Radical-Induced DNA Damage and Its Repair. A Chemical Perspective*; Springer: Berlin/Heidelberg, Germany, 2006.
2. Becker, D.; Adhikary, A.; Sevilla, M.D. Physicochemical mechanisms of radiation-induced DNA damage. In *Charged Particle and Photon Interactions with Matter. Recent Advances, Applications, and Interfaces*; Hatano, Y., Katsumura, Y., Mozumder, A., Eds.; CRC Press (Taylor & Francis Group): Boca Raton, FL, USA, 2011; Chapter 19, pp. 503–541.
3. Cadet, J.; Davies, K.J.A.; Medeiros, M.H.; Di Mascio, P.; Wagner, J.R. Formation and repair of oxidatively generated damage in cellular DNA. *Free Radic. Biol. Med.* **2017**, *107*, 13–34. [[CrossRef](#)] [[PubMed](#)]
4. O’Neill, P. Radiation-induced damage in DNA. In *Radiation Chemistry: Present Status and Future Trends*; Jonah, C.D., Rao, B.S.M., Eds.; Elsevier: Amsterdam, The Netherlands, 2001; Chapter 21; pp. 585–622.
5. Azzam, E.I.; Jay-Gerin, J.-P.; Pain, D. Ionizing radiation-induced metabolic oxidative stress and prolonged cell injury. *Cancer Lett.* **2012**, *327*, 48–60. [[CrossRef](#)] [[PubMed](#)]
6. Priyadarsini, K.I. Redox reactions of antioxidants: Contributions from radiation chemistry of aqueous solutions. In *Charged Particle and Photon Interactions with Matter. Recent Advances, Applications, and Interfaces*; Hatano, Y., Katsumura, Y., Mozumder, A., Eds.; CRC Press (Taylor & Francis Group): Boca Raton, FL, USA, 2011; Chapter 22, pp. 595–622.
7. Hall, E.J.; Giaccia, A.J. *Radiobiology for the Radiologist*, 8th ed.; Wolters Kluwer: Philadelphia, PA, USA, 2019.
8. Penabè, S.; Meesungnoen, J.; Jay-Gerin, J.-P. Assessment of cystamine’s radioprotective/antioxidant ability under high-dose-rate irradiation: A Monte Carlo multi-track chemistry simulation study. *Antioxidants* **2023**, *12*, 776. [[CrossRef](#)]
9. Favaudon, V.; Caplier, L.; Monceau, V.; Pouzoulet, F.; Sayarath, M.; Fouillade, C.; Poupon, M.-F.; Brito, I.; Hupé, P.; Bourhis, J.; et al. Ultrahigh dose-rate FLASH irradiation increases the differential response between normal and tumor tissue in mice. *Sci. Transl. Med.* **2014**, *6*, 245ra93. [[CrossRef](#)]
10. Favaudon, V.; Fouillade, C.; Vozenin, M.-C. La radiothérapie FLASH pour épargner les tissus sains. *Médecine/Sciences* **2015**, *31*, 121–123. [[CrossRef](#)] [[PubMed](#)]

11. Wilson, J.D.; Hammond, E.M.; Higgins, G.S.; Petersson, K. Ultra-high dose rate (FLASH) radiotherapy: Silver bullet or fool's gold? *Front. Oncol.* **2020**, *9*, 1563. [[CrossRef](#)]
12. Esplen, N.; Mendonca, M.S.; Bazalova-Carter, M. Physics and biology of ultrahigh dose-rate (FLASH) radiotherapy: A topical review. *Phys. Med. Biol.* **2020**, *65*, 23TR03. [[CrossRef](#)]
13. Wardman, P. Radiotherapy using high-intensity pulsed radiation beams (FLASH): A radiation-chemical perspective. *Radiat. Res.* **2020**, *194*, 607–617. [[CrossRef](#)]
14. Marcu, L.G.; Bezak, E.; Peukert, D.D.; Wilson, P. Translational research in FLASH radiotherapy—From radiobiological mechanisms to in vivo results. *Biomedicines* **2021**, *9*, 181. [[CrossRef](#)]
15. Vozenin, M.-C.; Bourhis, J.; Durante, M. Towards clinical translation of FLASH radiotherapy. *Nature Rev. Clin. Oncol.* **2022**, *19*, 791–803. [[CrossRef](#)]
16. Gao, Y.; Liu, R.; Chang, C.-W.; Charyyev, S.; Zhou, J.; Bradley, J.D.; Liu, T.; Yang, X. A potential revolution in cancer treatment: A topical review of FLASH radiotherapy. *J. Appl. Clin. Med. Phys.* **2022**, *23*, e13790. [[CrossRef](#)] [[PubMed](#)]
17. Kacem, H.; Almeida, A.; Cherbuin, N.; Vozenin, M.-C. Understanding the FLASH effect to unravel the potential of ultra-high dose rate irradiation. *Int. J. Radiat. Biol.* **2022**, *98*, 506–516. [[CrossRef](#)]
18. Schüller, E.; Acharya, M.; Montay-Gruel, P.; Loo, B.W., Jr.; Vozenin, M.-C.; Maxim, P.G. Ultra-high dose rate electron beams and the FLASH effect: From preclinical evidence to a new radiotherapy paradigm. *Med. Phys.* **2022**, *49*, 2082–2095. [[CrossRef](#)]
19. Friedl, A.A.; Prise, K.M.; Butterworth, K.T.; Montay-Gruel, P.; Favaudon, V. Radiobiology of the FLASH effect. *Med. Phys.* **2022**, *49*, 1993–2013. [[CrossRef](#)] [[PubMed](#)]
20. Hageman, E.; Che, P.-P.; Dahele, M.; Slotman, B.J.; Sminia, P. Radiobiological aspects of FLASH radiotherapy. *Biomolecules* **2022**, *12*, 1376. [[CrossRef](#)]
21. Jay-Gerin, J.-P. Ultra-high dose-rate (FLASH) radiotherapy: Generation of early, transient, strongly acidic spikes in the irradiated tumor environment. *Cancer Radiother.* **2020**, *24*, 332–334. [[CrossRef](#)] [[PubMed](#)]
22. Sultana, A.; Alanazi, A.; Meesungnoen, J.; Jay-Gerin, J.-P. Generation of ultrafast, transient, highly acidic pH spikes in the radiolysis of water at very high dose rates: Relevance for FLASH radiotherapy. *Can. J. Chem.* **2022**, *100*, 272–279. [[CrossRef](#)]
23. Loh, Z.-H.; Doumy, G.; Arnold, C.; Kjellsson, L.; Southworth, S.H.; Al Haddad, A.; Kumagai, Y.; Tu, M.-F.; Ho, P.J.; March, A.M.; et al. Observation of the fastest chemical processes in the radiolysis of water. *Science* **2020**, *367*, 179–182. [[CrossRef](#)]
24. Spinks, J.W.T.; Woods, R.J. *An Introduction to Radiation Chemistry*, 3rd ed.; Wiley: New York, NY, USA, 1990.
25. Garrett, B.C.; Dixon, D.A.; Camaioni, D.M.; Chipman, D.M.; Johnson, M.A.; Jonah, C.D.; Kimmel, G.A.; Miller, J.H.; Rescigno, T.N.; Rossky, P.J.; et al. Role of water in electron-initiated processes and radical chemistry: Issues and scientific advances. *Chem. Rev.* **2005**, *105*, 355–390. [[CrossRef](#)]
26. Cobut, V.; Frongillo, Y.; Jay-Gerin, J.-P.; Patau, J.P. A Monte Carlo calculation of subexcitation and vibrationally-relaxing electron spectra in irradiated liquid water. *Radiat. Phys. Chem.* **1992**, *40*, 589–591. [[CrossRef](#)]
27. LaVerne, J.A.; Pimblott, S.M. Electron energy-loss distributions in solid, dry DNA. *Radiat. Res.* **1995**, *141*, 208–215. [[CrossRef](#)]
28. Meesungnoen, J.; Jay-Gerin, J.-P.; Filali-Mouhim, A.; Mankhetkorn, S. Low-energy electron penetration range in liquid water. *Radiat. Res.* **2002**, *158*, 657–660. [[CrossRef](#)] [[PubMed](#)]
29. LaForge, A.C.; Michiels, R.; Bohlen, M.; Callegari, C.; Clark, A.; von Conta, A.; Coreno, M.; Di Fraia, M.; Drabbels, M.; Huppert, M.; et al. Real-time dynamics of the formation of hydrated electrons upon irradiation of water clusters with extreme ultraviolet light. *Phys. Rev. Lett.* **2019**, *122*, 133001. [[CrossRef](#)]
30. Low, P.J.; Chu, W.; Nie, Z.; Mohd Yusof, M.S.B.; Prezhdo, O.V.; Loh, Z.-H. Observation of a transient intermediate in the ultrafast relaxation dynamics of the excess electron in strong-field-ionized liquid water. *Nature Commun.* **2022**, *13*, 7300. [[CrossRef](#)] [[PubMed](#)]
31. Lea, D.E. *Actions of Radiations on Living Cells*; Cambridge University Press: Cambridge, UK, 1946; Chapter 2.
32. Lea, D.E. The action of radiations on dilute aqueous solutions: The spatial distribution of H and OH. *Br. J. Radiol.* **1947**, *1*, 59–64.
33. Morrison, P. Radiation in living matter: The physical processes. In *Symposium on Radiobiology. The Basic Aspects of Radiation Effects on Living Systems*; Nickson, J.J., Ed.; Wiley: New York, NY, USA, 1952; pp. 1–12.
34. Elliot, A.J.; Bartels, D.M. *The Reaction Set, Rate Constants and g-Values for the Simulation of the Radiolysis of Light Water over the Range 20 to 350 °C Based on Information Available in 2008*; Report No. 153-127160-450-001; Atomic Energy of Canada Limited: Mississauga, ON, Canada, 2009.
35. Kanike, V.; Meesungnoen, J.; Jay-Gerin, J.-P. Transient acid pH effect in tracks in the radiolysis of water: Does this effect contribute to biological damage caused by ionizing radiation? *Austin J. Nucl. Med. Radiother.* **2015**, *2*, 1011.
36. Kanike, V.; Meesungnoen, J.; Jay-Gerin, J.-P. Acid spike effect in spurs/tracks of the low/high linear energy transfer radiolysis of water: Potential implications for radiobiology. *RSC Adv.* **2015**, *5*, 43361–43370. [[CrossRef](#)]
37. LaVerne, J.A. Track effects of heavy ions in liquid water. *Radiat. Res.* **2000**, *153*, 487–496. [[CrossRef](#)]
38. Smith, D.R.; Stevens, W.H. Radiation-induced hydrolysis of acetal: Evidence for the reaction of H<sub>3</sub>O<sup>+</sup> ions in spurs in the radiolysis of water. *Nature* **1963**, *200*, 66–67. [[CrossRef](#)]
39. Anbar, M.; Thomas, J.K. Pulse radiolysis studies of aqueous sodium chloride solutions. *J. Phys. Chem.* **1964**, *68*, 3829–3835. [[CrossRef](#)]
40. Pikaev, A.K.; Kabakchi, S.A.; Zansokhova, A.A. Yields and reactions of hydrogen ions on radiolysis of water and aqueous solutions. *Faraday Discuss. Chem. Soc.* **1977**, *63*, 112–123. [[CrossRef](#)]

41. Byakov, V.M.; Stepanov, S.V. The mechanism for the primary biological effects of ionizing radiation. *Phys. Usp.* **2006**, *49*, 469–487. [[CrossRef](#)]
42. Kanike, V. “Acid-Spike” Effect in Spurs/Tracks of the Low/High Linear Energy Transfer Radiolysis of Water: Potential Implications for Radiobiology and Nuclear Industry. Master’s Thesis, Université de Sherbrooke, Sherbrooke, QC, Canada, 2016. Available online: <https://savoirs.usherbrooke.ca/handle/11143/9711> (accessed on 17 November 2016).
43. Islam, M.M.; Kanike, V.; Meesungnoen, J.; Lertnaisat, P.; Katsumura, Y.; Jay-Gerin, J.-P. In Situ generation of ultrafast transient “acid spikes” in the  $^{10}\text{B}(n,\alpha)^7\text{Li}$  radiolysis of water. *Chem. Phys. Lett.* **2018**, *693*, 210–215. [[CrossRef](#)]
44. Schneider, N.M.; Norton, M.M.; Mendel, B.J.; Grogan, J.M.; Ross, F.M.; Bau, H.H. Electron-water interactions and implications for liquid cell electron microscopy. *J. Phys. Chem. C* **2014**, *118*, 22373–22382. [[CrossRef](#)]
45. Platzman, R.L. The physical and chemical basis of mechanisms in radiation biology. In *Radiation Biology and Medicine. Selected Reviews in the Life Sciences*; Claus, W.D., Ed.; Addison-Wesley: Reading, MA, USA, 1958; pp. 15–72.
46. Kuppermann, A. Theoretical foundations of radiation chemistry. *J. Chem. Educ.* **1959**, *36*, 279–285. [[CrossRef](#)]
47. Meesungnoen, J.; Jay-Gerin, J.-P. Radiation chemistry of liquid water with heavy ions: Monte Carlo simulation studies. In *Charged Particle and Photon Interactions with Matter. Recent Advances, Applications, and Interfaces*; Hatano, Y., Katsumura, Y., Mozumder, A., Eds.; CRC Press (Taylor & Francis Group): Boca Raton, FL, USA, 2011; Chapter 14, pp. 355–400.
48. Ferradini, C.; Jay-Gerin, J.-P. Radiolysis of water and aqueous solutions: History and present state of the science. *Can. J. Chem.* **1999**, *77*, 1542–1575. (In French) [[CrossRef](#)]
49. Magee, J.L. Radiation chemistry. *Annu. Rev. Nucl. Sci.* **1953**, *3*, 171–192. [[CrossRef](#)]
50. Freeman, G.R. Basics of radiation chemistry. In *The Study of Fast Processes and Transient Species by Electron Pulse Radiolysis*; Baxendale, J.H., Busi, F., Eds.; Reidel Publishing: Dordrecht, The Netherlands, 1982; pp. 19–34.
51. Plante, I.L.; Filali-Mouhim, A.; Jay-Gerin, J.-P. SIMULRAD: A JAVA interface for a Monte Carlo simulation code to visualize in 3D the early stages of water radiolysis. *Radiat. Phys. Chem.* **2005**, *72*, 173–180. [[CrossRef](#)]
52. Mozumder, A. *Fundamentals of Radiation Chemistry*; Academic Press: San Diego, CA, USA, 1999.
53. Sanguanmith, S.; Meesungnoen, J.; Muroya, Y.; Lin, M.; Katsumura, Y.; Jay-Gerin, J.-P. On the spur lifetime and its temperature dependence in the low linear energy transfer radiolysis of water. *Phys. Chem. Chem. Phys.* **2012**, *14*, 16731–16736. [[CrossRef](#)]
54. Buxton, G.V. Radiation chemistry of the liquid state: (1) Water and homogeneous aqueous solutions. In *Radiation Chemistry. Principles and Applications*; Farhataziz, Rodgers, M.A.J., Eds.; VCH Publishers: New York, NY, USA, 1987; pp. 321–349.
55. Bjergbakke, E.; Hart, E.J. Oxygen formation in the  $\gamma$ -ray irradiation of  $\text{Fe}^{2+}$ - $\text{Cu}^{2+}$  solutions. *Radiat. Res.* **1971**, *45*, 261–273. [[CrossRef](#)]
56. Pastina, B.; LaVerne, J.A. Effect of molecular hydrogen on hydrogen peroxide in water radiolysis. *J. Phys. Chem. A* **2001**, *105*, 9316–9322. [[CrossRef](#)]
57. Ferradini, C. Heterogeneous aspect of radiolytic phenomena (Article in French). In *Actions Biologique et Chimique des Radiations Ionisantes*; Tilquin, B., Ed.; Éditions Ciaco: Brussels, Belgium, 1990; Volume 1, pp. 52–63.
58. Alanazi, A.; Meesungnoen, J.; Jay-Gerin, J.-P. Linear energy transfer dependence of transient yields in water irradiated by 150 keV–500 MeV protons in the limit of low dose rates. *Can. J. Chem.* **2020**, *98*, 427–433. [[CrossRef](#)]
59. Watt, D.E. *Quantities for Dosimetry of Ionizing Radiations in Liquid Water*; Taylor & Francis: London, UK, 1996.
60. *Stopping Powers and Ranges for Protons and Alpha Particles*; ICRU Report No. 49; International Commission on Radiation Units and Measurements: Bethesda, DC, USA, 1993.
61. Mustaree, S.; Meesungnoen, J.; Butarbutar, S.L.; Causey, P.; Stuart, C.R.; Jay-Gerin, J.-P. Self-radiolysis of tritiated water. 3. The  $\bullet\text{OH}$  scavenging effect of bromide ions on the yield of  $\text{H}_2\text{O}_2$  in the radiolysis of water by  $^{60}\text{Co}$   $\gamma$ -rays and tritium  $\beta$ -particles at room temperature. *RSC Adv.* **2014**, *4*, 43572–43581. [[CrossRef](#)]
62. Alanazi, A.; Meesungnoen, J.; Jay-Gerin, J.-P. A computer modeling study of water radiolysis at high dose rates. Relevance to FLASH radiotherapy. *Radiat. Res.* **2021**, *195*, 149–162. [[CrossRef](#)]
63. Sultana, A.; Alanazi, A.; Meesungnoen, J.; Jay-Gerin, J.-P. On the transient radiolytic oxygen depletion in the ultra-high (FLASH) dose-rate radiolysis of water in a cell-like environment: Effect of  $\text{e}^-_{\text{aq}}$  and  $\bullet\text{OH}$  competing scavengers. *Radiat. Res.* **2022**, *197*, 566–567. [[CrossRef](#)]
64. Alanazi, A.; Sultana, A.; Meesungnoen, J.; Jay-Gerin, J.-P. The effect of linear energy transfer on the early, transient radiolytic oxygen depletion in the radiolysis of water by high-dose-rate irradiating protons. *Can. J. Chem.* **2023**, *101*, 70–80. [[CrossRef](#)]
65. Sultana, A.; Meesungnoen, J.; Jay-Gerin, J.-P. High-dose-rate effects in the radiolysis of water at elevated temperatures. *Can. J. Chem.* **2021**, *99*, 594–602. [[CrossRef](#)]
66. *The Dosimetry of Pulsed Radiation*; ICRU Report No. 34; International Commission on Radiation Units and Measurements: Bethesda, MD, USA, 1982.
67. Cobut, V.; Frongillo, Y.; Patau, J.P.; Goulet, T.; Fraser, M.-J.; Jay-Gerin, J.-P. Monte Carlo simulation of fast electron and proton tracks in liquid water—I. Physical and physicochemical aspects. *Radiat. Phys. Chem.* **1998**, *51*, 229–243.
68. Frongillo, Y.; Goulet, T.; Fraser, M.-J.; Cobut, V.; Patau, J.P.; Jay-Gerin, J.-P. Monte Carlo simulation of fast electron and proton tracks in liquid water—II. Nonhomogeneous chemistry. *Radiat. Phys. Chem.* **1998**, *51*, 245–254.
69. Tachiya, M. Theory of diffusion-controlled reactions: Formulation of the bulk reaction rate in terms of the pair probability. *Radiat. Phys. Chem.* **1983**, *21*, 167–175. [[CrossRef](#)]

70. Pimblott, S.M.; Pilling, M.J.; Green, N.J.B. Stochastic models of spur kinetics in water. *Radiat. Phys. Chem.* **1991**, *37*, 377–388. [[CrossRef](#)]
71. Goulet, T.; Fraser, M.-J.; Frongillo, Y.; Jay-Gerin, J.-P. On the validity of the independent reaction times approximation for the description of the nonhomogeneous kinetics of liquid water radiolysis. *Radiat. Phys. Chem.* **1998**, *51*, 85–91. [[CrossRef](#)]
72. Plante, I. Développement de Codes de Simulation Monte Carlo de la Radiolyse de l'Eau par des Électrons, Ions Lourds, Photons et Neutrons. Applications à Divers Sujets d'Intérêt Expérimental. Ph.D. Thesis, Université de Sherbrooke, Sherbrooke, QC, Canada, 2009.
73. Tippayamontri, T.; Sunuchakan, S.; Meesungnoen, J.; Sunaryo, G.R.; Jay-Gerin, J.-P. Fast neutron radiolysis of the ferrous sulfate (Fricke) dosimeter: Monte Carlo simulations. In *Recent Research Developments in Physical Chemistry*; Pandalai, S.G., Ed.; Transworld Research Network: Trivandrum, Kerala, India, 2009; Volume 10, pp. 143–211.
74. Mirsaleh Kohan, L.; Sanguanmith, S.; Meesungnoen, J.; Causey, P.; Stuart, C.R.; Jay-Gerin, J.-P. Self-radiolysis of tritiated water. 1. A comparison of the effects of  $^{60}\text{Co}$   $\gamma$ -rays and tritium  $\beta$ -particles on water and aqueous solutions at room temperature. *RSC Adv.* **2013**, *3*, 19282–19299. [[CrossRef](#)]
75. Čerček, B.; Kongshaug, M. Hydrogen ion yields in the radiolysis of neutral aqueous solutions. *J. Phys. Chem.* **1969**, *73*, 2056–2058. [[CrossRef](#)] [[PubMed](#)]
76. Barker, G.C.; Fowles, P.; Sammon, D.C.; Stringer, B. Pulse radiolytic induced transient electrical conductance in liquid solutions. Part 1. Technique and the radiolysis of water. *Trans. Faraday Soc.* **1970**, *66*, 1498–1508. [[CrossRef](#)]
77. Anderson, R.F.; Vojnovic, B.; Michael, B.D. The radiation-chemical yields of  $\text{H}_3\text{O}^+$  and  $\text{OH}^-$  as determined by nanosecond conductimetric measurements. *Radiat. Phys. Chem.* **1985**, *26*, 301–303. [[CrossRef](#)]
78. Schmidt, K.H.; Ander, S.M. Formation and recombination of  $\text{H}_3\text{O}^+$  and hydroxide in irradiated water. *J. Phys. Chem.* **1969**, *73*, 2846–2852. [[CrossRef](#)]
79. Kuppermann, A. Diffusion kinetics in radiation chemistry. In *Actions Chimiques et Biologiques des Radiations*; Haïssinsky, M., Ed.; Masson: Paris, France, 1961; Volume 5, pp. 85–166.
80. Hummel, A. *Radiation Chemistry: The Chemical Effects of Ionizing Radiation and their Applications*; Interfaculty Reactor Institute-Technische Universiteit Delft (IRI-FUT): Delft, The Netherlands, 1995.
81. Schardt, D.; Elsässer, T.; Schulz-Ertner, D. Heavy-ion tumor therapy: Physical and radiobiological benefits. *Rev. Mod. Phys.* **2010**, *82*, 383–425. [[CrossRef](#)]
82. Baverstock, K.F.; Burns, W.G. Primary production of oxygen from irradiated water as an explanation for decreased radiobiological oxygen enhancement at high LET. *Nature* **1976**, *260*, 316–318. [[CrossRef](#)]
83. Draganić, I.G.; Draganić, Z.D. *The Radiation Chemistry of Water*; Academic Press: New York, NY, USA, 1971.
84. Negendank, W.; Edelman, L. *The State of Water in the Cell*; Scanning Microscopy International: Chicago, IL, USA, 1988.
85. Swietach, P.; Vaughan-Jones, R.D. Relationship between intracellular pH and proton mobility in rat and guinea-pig ventricular myocytes. *J. Physiol.* **2005**, *566*, 793–806. [[CrossRef](#)]

**Disclaimer/Publisher's Note:** The statements, opinions and data contained in all publications are solely those of the individual author(s) and contributor(s) and not of MDPI and/or the editor(s). MDPI and/or the editor(s) disclaim responsibility for any injury to people or property resulting from any ideas, methods, instructions or products referred to in the content.